Research Article | Vol. 24, No. 24 | 28 Nov 2016 | OPTICS EXPRESS 27726

Optics EXPRESS

Intra-half-cycle interference of low-energy photoelectron in strong midinfrared laser fields

HUI XIE,[1] MIN LI,[1,*] YANG LI,[1] YUEMING ZHOU,[1] AND PEIXIANG LU[1,2,3]

[1]*Wuhan National Laboratory for Optoelectronics and School of Physics, Huazhong University of Science and Technology, Wuhan 430074, China*
[2]*Laboratory of Optical Information Technology, Wuhan Institute of Technology, Wuhan 430205, China*
[3]*lupeixiang@hust.edu.cn*
[*]*mli@hust.edu.cn*

Abstract: Using semiclassical models with implementing interference effects, we study the low-energy photoelectron intra-half-cycle interferences among nonscattering trajectories and multiple forward scattering trajectories of atoms ionized by a strong mid-infrared laser field. Tracing back to the initial tunneling coordinates, we find that up to three kinds of forward scattering trajectories have substantial contributions to the low-energy photoelectrons. Those multiple forward scattering trajectories depend sensitively on the initial transverse momentum at the tunnel exit and they lead to sign reversal of the transverse momentum of the electrons. We show that the interference of the nonscattering trajectory and the triple-scattered trajectory has the largest contribution to the low-energy structure in mid-infrared laser fields. It is also shown that the long-range Coulomb potential has a significant effect on the low-energy photoelectron interference patterns.

OCIS codes: (020.2649) Strong field laser physics; (260.3230) Ionization; (270.6620) Strong-field processes.

References and links

1. P. B. Corkum and F. Krausz, "Attosecond science," Nature Phys. **3**(6), 381–387 (2007).
2. P. B. Corkum, "Plasma perspective on strong field multiphoton ionization," Phys. Rev. Lett. **71**(13), 1994 (1993).
3. M. B. Gaarde and K. J. Schafer, "Quantum path distributions for high-order harmonics in rare gas atoms," Phys. Rev. A **65**(3), 031406 (2002).
4. O. Smirnova, Y. Mairesse, S. Patchkovskii, N. Dudovich, D. Villeneuve, P. Corkum, and M. Y. Ivanov, "High harmonic interferometry of multi-electron dynamics in molecules," Nature **460**(7258), 972–977 (2009).
5. C. Zhai, L. He, P. Lan, X. Zhu, Y. Li, F. Wang, W. Shi, Q. Zhang, and P. Lu, "Coulomb-corrected molecular orbital tomography of nitrogen," Sci. Rep. **6**, 23236 (2016).
6. X. Zhu, P. Lan, K. Liu, Y. Li, X. Liu, Q. Zhang, I. Barth, and P. Lu, "Helicity sensitive enhancement of strong-field ionization in circularly polarized laser fields," Opt. Express **24**(4), 4196–4209 (2016).
7. J. S. Parker, B. J. S. Doherty, K. T. Taylor, K. D. Schultz, C. I. Blaga, and L. F. DiMauro, "High-energy cutoff in the spectrum of strong-field nonsequential double ionization," Phys. Rev. Lett. **96**(13), 133001 (2006).
8. X. Ma, Y. Zhou, and P. Lu, "Multiple recollisions in strong-field nonsequential double ionization," Phys. Rev. A **93**(1), 013425 (2016).
9. A. Tong, Y. Zhou, and P. Lu, "Resolving subcycle electron emission in strong-field sequential double ionization," Opt. Express **23**(12), 15774–15783 (2015).
10. Z. Wang, M. Li, Y. Zhou, Y. Li, P. Lan, and P. Lu, "Counterintuitive energy shifts in joint electron-nuclear-energy spectra of strong-field fragmentation of H_2^+," Phys. Rev. A **93**(1), 013418 (2016).
11. M. Okunishi, R. Itaya, K. Shimada, G. Prumper, K. Ueda, M. Busuladzic, A. G. Busuladzic, D. B. Milosevic, and W. Becker, "Two-source double-slit interference in angle-resolved high-energy above-threshold ionization spectra of diatoms," Phys. Rev. Lett. **103**(4), 043001 (2009).
12. C. C. Chirilă and M. Lein, "High-order above-threshold ionization in stretched molecules," Phys. Rev. A **74**(5), 051401 (2006).
13. C. Altucci, V. Tosa, R. Velotta, and C. H. Nam, "Dynamical medium depletion in high-order above-threshold ionization with few-cycle laser pulses," Phys. Rev. A **70**(6), 065402 (2004).
14. D. B. Milošević ,W. Becker, M. Okunishi, G. Prümper, K. Shimada, and K. Ueda, "Strong-field electron spectra of rare-gas atoms in the rescattering regime: enhanced spectral regions and a simulation of the experiment," J. Phys. B: At. Mol. Opt. Phys. **43**(1), 015401 (2010).
15. C. I. Blaga, F. Catoire, P. Colosimo, G. G. Paulus, H. G. Muller, P. Agostini, and L. F. DiMauro, "Strong-field photoionization revisited," Nat. Phys. **5**(5), 335–338 (2009).

#279216 http://dx.doi.org/10.1364/OE.24.027726
Journal © 2016 Received 20 Oct 2016; revised 15 Nov 2016; accepted 15 Nov 2016; published 18 Nov 2016

Optics EXPRESS

16. W. Quan, Z. Lin, M. Wu, H. Kang, H. Liu, X. Liu, J. Chen, J. Liu, X. T. He, S. G. Chen, H. Xiong, L. Guo, H. Xu, Y. Fu, Y. Cheng, and Z. Z. Xu, "Classical aspects in above-threshold ionization with a midinfrared strong laser field," Phys. Rev. Lett. **103**(9), 093001 (2009).
17. C. Lemell, J. Burgdörfer, S. Gräfe, K. I. Dimitriou, D. G. Arbó, and X.-M. Tong, "Classical-quantum correspondence in atomic ionization by midinfrared pulses: multiple peak and interference structures," Phys. Rev. A **87**(1), 013421 (2013).
18. F. H. M. Faisal, "Strong-field physics: ionization surprise," Nat. Phys. **5**(5), 319–320 (2009).
19. C. Liu and K. Z. Hatsagortsyan, "Origin of unexpected low energy structure in photoelectron spectra induced by midinfrared strong laser fields," Phys. Rev. Lett. **105**(11), 113003 (2010).
20. T. M. Yan, S. V. Popruzhenko, M. J. J. Vrakking, and D. Bauer, "Low-energy structures in strong field ionization revealed by quantum orbits," Phys. Rev. Lett. **105**(25), 253002 (2010).
21. D. A. Telnov and S.-I. Chu, "Low-energy structure of above-threshold-ionization electron spectra: Role of the Coulomb threshold effect," Phys. Rev. A **83**(6), 063406 (2011).
22. A. Kästner, U. Saalmann, and J. M. Rost, "Electron-energy bunching in laser-driven soft recollisions," Phys. Rev. Lett. **108**(3), 033201 (2012).
23. L. Guo, S. S. Han, X. Liu, Y. Cheng, Z. Z. Xu, J. Fan, J. Chen, S. G. Chen, W. Becker, C. I. Blaga, A. D. DiChiara, E. Sistrunk, P. Agostini, and L. F. DiMauro, "Scaling of the low-energy structure in above-threshold ionization in the tunneling regime: theory and experiment," Phys. Rev. Lett. **110** (1), 013001 (2013).
24. C. Y. Wu, Y. D. Yang, Y. Q. Liu, Q. H. Gong, M. Y. Wu, X. Liu, X. L. Hao, W. D. Li, X. T. He, and J. Chen, "Characteristic spectrum of very low-energy photoelectron from above-threshold ionization in the tunneling regime," Phys. Rev. lett. **109**(4), 043001 (2012).
25. J. Dura, N. Camus, A. Thai, A. Britz, M. Hemmer, M. Baudisch, A. Senftleben, C. D. Schröter, J. Ullrich, R. Moshammer, and J. Biegert, "Ionization with low-frequency fields in the tunneling regime," Sci. Rep.**3**, 2675 (2013).
26. M. Möller, F. Meyer, A. M. Sayler, G. G. Paulus, M. F. Kling, B. E. Schmidt, W. Becker, and D. B. Milošević, "Off-axis low-energy structures in above-threshold ionization," Phys. Rev. A **90**(2), 023412 (2014).
27. P. Agostini, F. Fabre, G. Mainfray, G. Petite, and N. K. Rahman, "Free-free transitions following six-photon ionization of xenon atoms," Phys. Rev. Lett. **42**(11), 1127 (1979).
28. M. Li, P. Zhang, S. Luo, Y. Zhou, Q. Zhang, P. Lan, and P. Lu, "Selective enhancement of resonant multiphoton ionization with strong laser fields," Phys. Rev. A **92**(6), 063404 (2015).
29. M. Li, J. W. Geng, H. Liu, Y. Deng, C. Wu, L. Y. Peng, Q. Gong, and Y. Liu, "Classical-quantum correspondence for above-threshold ionization," Phys. Rev. Lett. **112**(11), 113002 (2014).
30. D. G. Arbó, E. Persson and J. Burgdörfer, "Time double-slit interferences in strong-field tunneling ionization," Phys. Rev. A **74**(6), 063407 (2006).
31. X.-B. Bian, Y. Huismans, O. Smirnova, K.-J. Yuan, M. J. J. Vrakking, and A. D. Bandrauk,"Subcycle interference dynamics of time-resolved photoelectron holography with midinfrared laser pulses," Phys. Rev. A **84**(4), 043420 (2011).
32. F. Lindner, M. G. Schätzel, H. Walther, A. Baltuška, E. Goulielmakis, F. Krausz, D. B. Milošević, D. Bauer, W. Becker, and G. G. Paulus, "Attosecond double-slit experiment," Phys. Rev. Lett. **95**(4), 040401 (2005).
33. R. Gopal, K. Simeonidis, R. Moshammer, T. Ergler, M. Dürr, M. Kurka, K. U. Kühnel, S. Tschuch, C.-D. Schröter, D. Bauer, J. Ullrich, A. Rudenko, O. Herrwerth, T. Uphues, M. Schultze, E. Goulielmakis, M. Uiberacker, M. Lezius, and M. F. Kling, "Three-dimensional momentum imaging of electron wave packet interference in few-cycle laser pulses," Phys. Rev. Lett. **103**(5), 053001 (2009).
34. M. Richter, M. Kunitski, M. Schöffler, T. Jahnke, L. P. H. Schmidt, M. Li, Y. Liu, and R. Dörner, "Streaking temporal double-slit interference by an orthogonal two-color laser field," Phys. Rev. Lett. **114**(14), 143001 (2015).
35. X. Xie, S. Roither, D. Kartashov, E. Persson, D. G. Arbó, L. Zhang, S. Gräfe, M. S. Schöffler, J. Burgdörfer, A. Baltuška, and M. Kitzler, "Attosecond probe of valence-electron wave packets by subcycle sculpted laser fields," Phys. Rev. Lett. **108**(19), 193004(2012).
36. D. G. Arbó, K. L. Ishikawa, K. Schiessl, E. Persson, and J. Burgdörfer, "Intracycle and intercycle interferences in above-threshold ionization: the time grating," Phys. Rev. A **81**(2), 021403 (2010).
37. Y. Huismans, A. Rouzée, A. Gijsbertsen, J. H. Jungmann, A. S. Smolkowska, P. S. W. M. Logman, F. Lépine, C. Cauchy, S. Zamith, T. Marchenko, J. M. Bakker, G. Berden, B. Redlich, A. F. G. van der Meer, H. G. Muller, W. Vermin, K. J. Schafer, M. Spanner, M. Y. Ivanov, O. Smirnova, D. Bauer, S. V. Popruzhenko, and M. J. J. Vrakking, "Time-resolved holography with photoelectrons," Science **331**(6013), 61–64 (2011).
38. Y. Zhou, O. I. Tolstikhin, and T. Morishita, "Near-forward rescattering photoelectron holography in strong-field ionization: extraction of the phase of the scattering amplitude," Phys. Rev. Lett. **116**(17), 173001 (2016).
39. M. He, Y. Li, Y. Zhou, M. Li, and P. Lu, "Temporal and spatial manipulation of the recolliding wave packet in strong-field photoelectron holography," Phys. Rev. A **93**(3), 033406 (2016).
40. M.-M. Liu, M. Li, C. Wu, Q. Gong, A. Staudte, and Y. Liu, "Phase structure of strong-field tunneling wave packets from molecules," Phys. Rev. Lett. **116**(16), 163004 (2016).
41. X.-B. Bian and A. D. Bandrauk, "Attosecond time-resolved imaging of molecular structure by photoelectron holography," Phys. Rev. Lett. **108**(26), 263003 (2012).
42. M. Haertelt, X.-B. Bian, M. Spanner, A. Staudte, and P. B. Corkum, "Probing molecular dynamics by laser-induced backscattering holography," Phys. Rev. Lett. **116**(13), 133001 (2016).

Optics EXPRESS

43. D. D. Hickstein, P. Ranitovic, S. Witte, X. M. Tong, Y. Huismans, P. Arpin, X. Zhou, K. E. Keister, C. W. Hogle, B. Zhang, C. Ding, P. Johnsson, N. Toshima, M. J. J. Vrakking, M. M. Murnane, and H. C. Kapteyn, "Direct visualization of laser-driven electron multiple scattering and tunneling distance in strong-field ionization," Phys. Rev. Lett. **109**(7), 073004 (2012).
44. L. D. Landau and E. M. Lifschitz, *Quantum Mechanics (Non-Relativisitic Theory)* (Oxford University, 1958).
45. M. V. Ammosov, N. B. Delone, and V. P. Krainov, "Tunnel ionization of complex atoms and of atomic ions in an alternating electromagnetic field," Zh. Eksp. Teor. Fiz. **91**(6), 2008(1986), [Sov. Phys. JETP **64**(6), 1191–1194 (1986)].
46. N. B. Delone and V. P. Krainov, "Energy and angular electron spectra for the tunnel ionization of atoms by strong low-frequency radiation," J. Opt. Soc. Am. B **8**(6), 1207–1211 (1991).
47. N. I. Shvetsov-Shilovski, M. Lein, L. B. Madsen, E. Räsänen, C. Lemell, J. Burgdörfer, D. G. Arbó, and K. Tőkési, "Semiclassical two-step model for strong-field ionization," Phys. Rev. A **94**(1), 013415 (2016).
48. T. Nubbemeyer, K. Gorling, A. Saenz, U. Eichmann, and W. Sandner, "Strong-field tunneling without ionization," Phys. Rev. Lett. **101**(23), 233001 (2008).

1. Introduction

The dynamics of electrons ionized by a strong laser field from atoms or molecules are often described by the classical three-step model [1, 2]. In this model, electron will firstly be tunnel ionized and then be accelerated in the laser field. With the change of electric field direction, the electron may return to the nucleus, leading to high-order harmonic generation (HHG) with electron recombination [3–6], nonsequential double ionization with inelastic scattering [7–10], high-order above-threshold ionization with elastic scattering [11–14], *etc*.

If an electron is scattered forward with a small scattering angle by the nucleus, it may contribute to the low-energy structures (LES) [15–17]. The observation of LES in a mid-infrared laser field has been regarded as an "ionization surprise" in strong-field physics [18]. All theoretical interpretations agree that the forward scattering of the photoelectrons is responsible for the low-energy structures [19–23]. Subsequently, the very-low energy structure [24], the near-zero energy structure [25], and the off-axis low-energy structure are experimentally reported [26]. Those previous studies mostly focus on the classical aspect of the LES, neglecting the interference effect among the electron wave packets.

In fact, electrons released at different phases of the laser field will give rise to the interference effect when the final momenta are the same. Neglecting the rescattering effect, there are two general types of photoelectron interference in a laser pulse. The first type is the intercycle interference with electron wave packets released at time intervals separated by the laser cycles, which leads to the well-known above-threshold ionization (ATI) structure with equidistant peaks in the energy spectrum [27–29]. The second type is the intracycle interference with electron wave packets released from adjacent half cycles. For this type of interference, one trajectory is ionized directly (direct trajectory) and another one reverses its direction in the laser field (indirect trajectory) [30, 31]. The intracycle interference between the direct and indirect trajectories is firstly observed in a carrier-envelope phase stabilized few-cycle laser pulse [32, 33], which is also known as a temporal double-slit interference. Recently, it is reported that this temporal double-slit interference can be streaked by a phase-controlled two-color laser field [34–36].

Considering the rescattering effect, more interference channels will contribute to the final photoelectron angular distributions (PADs). Huismans *et al.* reported the famous spiderlike structure using a laser pulse with a wavelength of 7000 nm [37]. This spiderlike structure arises from the interference between the forward scattering trajectory and the nonscattering trajectory, thus it is known as a kind of forward scattering photoelectron holography. This forward scattering photoelectron holography can be used to retrieve the phase of the scattering amplitude of atoms and the phase structure of electron wave packets from tunneling ionization of molecules [38–40]. Bian *et al.* theoretically predicted the backward scattering photoelectron holographic structure by solving the time-dependent Schrödinger equation of H_2^+, which was confirmed by recent experiments [41, 42]. Furthermore, Hickstein and co-workers found a different spider-like struc-

Optics EXPRESS

ture in the low-energy region which is dubbed as inner spider structures [43]. They used a plane-spherical-wave interference model to explain this inner spider structure, in which the effect of the long-range Coulomb potential is ignored. Using this perturbative model, they show that the inner spider structure comes from the interference of unscattered trajectories and trajectories scattered at their second revisit to the nucleus. Because the plane-spherical-wave model depends on many empirical parameters, up to now the electron trajectories that contribute to the inner spider structure is not resolved. The photoelectron interference effect for the LES is not completely clear.

On the other hand, many previous studies have neglected the effect of the long-range Coulomb potential on the photoelectron interference [30,43]. However the long-range Coulomb potential has shown its importance on the electron trajectories, especially for the low-energy photoelectrons [16,17,19,24]. Thus it is highly necessary to study the effect of atomic Coulomb potential on the low-energy photoelectron interference structure.

In this paper, we study the PADs of atoms ionized by a mid-infrared laser field using the quantum-trajectory Monte Carlo (QTMC) [29] model and a semi-classical rescattering model. Both models are independent on empirical parameters. With the QTMC model, we reproduce the inner spider structure in the low energy region observed in the experiment [43]. We show that the inner spider structure comes from the interference between the multiple forward scattering trajectories and the nonscattering trajectories within a half cycle. Tracing back to the initial tunneling coordinates, we find that up to three kinds of forward scattering trajectories have a substantial contribution to the inner spider structure in low-energy region. Depending on the initial transverse momentum at the tunnel exit, those multiple forward scattering trajectories can interfere with the nonscattering trajectories. The interference patterns among the multiple forward scattering trajectories and the nonscattering trajectories are systematically studied. We show that the interference of the nonscattering trajectories and triple-scattered trajectories plays the most important role in the formation of the inner spider structure. We further study the effect of the Coulomb potential on the interference patterns by comparing the QTMC model with the semi-classical rescattering model.

2. Methods

2.1. Quantum trajectory Monte Carlo model

The details of the QTMC model are described in [29]. Briefly, in QTMC model the initial position of electrons are derived from the method in Landau's book [44], in which the Schrödinger equation is separated in parabolic coordinates for an electron in the static electric field. The tunneling ionization time and the initial transverse momentum distribution of electron wave packets are given by the Ammosov-Delone-Krainov (ADK) theory [45, 46]. The initial momentum along the laser polarization direction is set to be zero. The weight of each trajectory is given by $W(t_0, v_x) = W_0(t_0)W_1(v_x)$. Here $W_0(t_0) = \left|(2I_p)^2/|E_0(t_0)|\right|^{2/\sqrt{2I_p}-1}\exp[-2(2I_p)^{3/2}/|3E_0(t_0)|]$ and $W_1(v_x) \propto [\sqrt{2I_p}/|E_0(t_0)|]\exp[\sqrt{2I_p}(v_x)^2/|E_0(t_0)|]$, in which I_p is the ionization potential, v_x is the initial transverse momentum, and t_0 is the ionization time. In order to simplify the calculation we have used a two-dimensional model. Atomic units are used unless specified otherwise. After tunneling, the evolution of the electron is governed by the classical Newtonian equation, i.e., $d^2\mathbf{r}(t)/dt^2 = -\mathbf{E}(t) - \nabla \cdot V(\mathbf{r})$, where $V(\mathbf{r})$ is the Coulomb potential as a function of the spatial coordinates $\mathbf{r}$ of the electron. Simultaneously, each trajectory is encoded with a phase S_i, which is given by the action integral along the trajectory. This phase is further modified by N. I. Shvetsov-Shilovski *et al.* [47], which can be written as

Optics EXPRESS

$$S_i = -\mathbf{v}_0 \cdot \mathbf{r}(t_0) + I_p t_0 + \int_{t_0}^{\infty} \left\{ \mathbf{v}_i^2(t)/2 - 2Z/|\mathbf{r}(t)| \right\} dt, \tag{1}$$

where $\mathbf{v}_0$ is the initial velocity at the tunneling ionization time t_0, $\mathbf{v}_i(t)$ is the velocity of the ith electron in the combined Coulomb and laser fields and Z is the ionic charge.

In the simulation, the laser pulse is polarized along z-axis

$$E(t) = E_0 \cdot \sin(\omega t + \varphi) \cdot f(t) \cdot \hat{\mathbf{z}}, \tag{2}$$

where E_0 is the electric amplitude of the laser pulse, ω is the frequency of the pulse, φ is the carrier-envelope phase (Here we set $\varphi = 0$ because the carrier-envelope phase has no effect in our simulation) and $f(t)$ is the envelope of the laser pulse. The laser envelope is trapezoidal which has eight optical cycles in total with two cycles linearly ramping on and off

$$f(t) = \begin{cases} \dfrac{t}{2T}, & 0 < t \le 2T, \\ 1, & 2T < t \le 6T, \\ \dfrac{8T - t}{2T}, & 6T < t \le 8T, \end{cases} \tag{3}$$

where T is the optical cycle of the laser pulse.

2.2. Semi-classical rescattering model

In order to study the Coulomb effect on the interference patterns, we further use a semi-classical rescattering model without the long-range Coulomb potential to show the interference structures between nonscattering electron wave packet and multiple forward scattering electron wave packet. This model is based on the three-step recollision model and has included the interference effect of the electron trajectories [41,42]. Because it is difficult to separate the interference structures of different multiple forward scattering trajectories from each other in the QTMC model, we use the semi-classical rescattering model to obtain the separated interference structure.

Because the laser envelope has a minor effect on the intra-half-cycle interference structure in the semiclassical rescattering model, we assume that the laser field is sine-like plane wave, i.e., $E(t) = E_0 \sin(\omega t)$. Similar to optical holography, the nonscattering electron can be seen as a reference wave which released at t_0^{ref} and the forward scattering electrons can be seen as a signal wave released at t_0^{sig} after the field maximum of the laser pulse with zero initial momentum. The velocity of the electrons in the laser field before the rescattering can be written as

$$v_z = -\frac{E_0}{\omega}[\cos(\omega t) - \cos(\omega t_0)]. \tag{4}$$

The rescattering time t_c is obtained by solving the equation of motion,

$$\sin(\omega t_c) - \sin(\omega t_0^{sig}) - \omega(t_c - t_0^{sig})\cos(\omega t_0^{sig}) = 0. \tag{5}$$

At the instant of rescattering, the electron elastically scatters off the nucleus with a scattering angle θ_c with respect to the impact direction. For the multiple forward scattering trajectory, the scattering angle θ_c is zero until the last time forward scattering, because nonzero scattering angle will cause the electron to miss the nucleus at its next return. The scattering angle θ_c for the last forward scattering is within $[-90°, 90°]$. Thus, the final momentum of the rescattering trajectory is given by

$$\begin{aligned} p_z &= \frac{E_0}{\omega}\cos(\omega t_c) + v_c \cos(\theta_c), \\ p_x &= v_c \sin(\theta_c), \end{aligned} \tag{6}$$

Optics EXPRESS

where v_c is the electron velocity at the instant of rescattering.

For the ionization phase [102.5°, 180°], Eq. (5) has only one solution for the rescattering time t_c with $t_c < 1.25T$ which satisfies the scattering time of the single-scattered trajectory. Equation (5) has at least three solutions for the ionization phase within (90°, 102.5°). Those three solutions correspond to scattering time of the multiple forward scattering trajectories. For the double-scattered trajectory, the two scattering time t_c satisfies $t_c < 1.25T$ and $1.25T < t_c < 1.75T$, respectively. For the triple-scattered trajectory, the three scattering time t_c satisfies $t_c < 1.25T$, $1.25T < t_c < 1.75T$, and $1.75T < t_c < 2.25T$, respectively. Because in the semi-classical model the final momenta of the forward scattering trajectories and the nonscattering trajectories are the same, we can directly calculate the ionization time and the initial transverse momenta for the nonscattering trajectories

$$\begin{aligned} t_0^{ref} &= \frac{1}{\omega}[\pi - \cos^{-1}(\omega p_z/E_0)], \\ v_x &= p_x. \end{aligned} \tag{7}$$

The phase of each trajectory without considering the long-range Coulomb potential is $S = \int_{t_0}^{\infty}(\frac{v^2(t)}{2} + I_p)dt$. Therefore, the phase difference between the forward scattering trajectories and the nonscattering trajectories is,

$$\Delta S_0 = \frac{1}{2}\int_{t_0^{sig}}^{t_c} v_z^2 dt - \frac{1}{2}\int_{t_0^{ref}}^{t_c} v_z^2 dt - \frac{1}{2}v_x^2(t_c - t_0^{ref}) - I_p(t_0^{sig} - t_0^{ref}) \tag{8}$$

The interference patterns are determined by this phase difference, i.e., $W = \cos^2(\Delta S_0/2)$. In this model, we assume each pair of trajectories is weighted by the ADK theory [45, 46]. We have also sampled the electron ensemble with the Monte-Carlo method.

Compared with the QTMC model, we have neglected the long-range ionic Coulomb potential effect in this rescattering model. Thus the effect of the long-range Coulomb potential on the interference patterns can be directly revealed when we compare the interference patterns using those two models.

3. Results and discussions

We first use the QTMC method to study the photoelectron interferences in a midinfrared laser field. The laser pulse has an intensity of 4×10^{13} W/cm^2 and a wavelength of 2000 nm. The ponderomotive potential $U_p = E_0^2/4\omega^2$ of the pulse is 0.549 a.u. We show the simulated two-dimensional PADs by the QTMC model in Fig. 1(a). Because the ionization during the ramp-on and ramp-off of the laser pulse has a minor contribution to the PADs, we only sample the electrons in the plateau of the pulse, as shown by the red area at the top of Fig. 1(a). We can see that the overall distributions look very similar to the experimental results at similar laser conditions [26,43]. The PADs reveal many interference patterns. Firstly, the PADs display many ring-like interference patterns centered around zero momentum, which corresponds to the ATI peak in the energy spectrum. Those interference patterns come from the intercycle interference of electron wave packets. Secondly, within each ring-like structure, there are many spot-like structures. Those structures arise from the intracycle interference among the direct trajectories, the indirect trajectories, and the rescattering trajectories [29]. Interesting, in the low energy region, the PADs show a finger-like interference structure, which is dramatically different with the higher-energy photoelectron. Those patterns has been experimentally observed in [26, 43].

Benefiting from the the advantage of the QTMC model, we can sample the electrons within a half cycle of the pulse to study the intra-half-cycle interference of the electron wave packet. Figure 1(b) shows the simulated two-dimensional PADs which is ionized within a half cycle of the laser pulse, i.e., [2T, 2.5T]. All the interference structures come from the intra-half-cycle

Optics EXPRESS

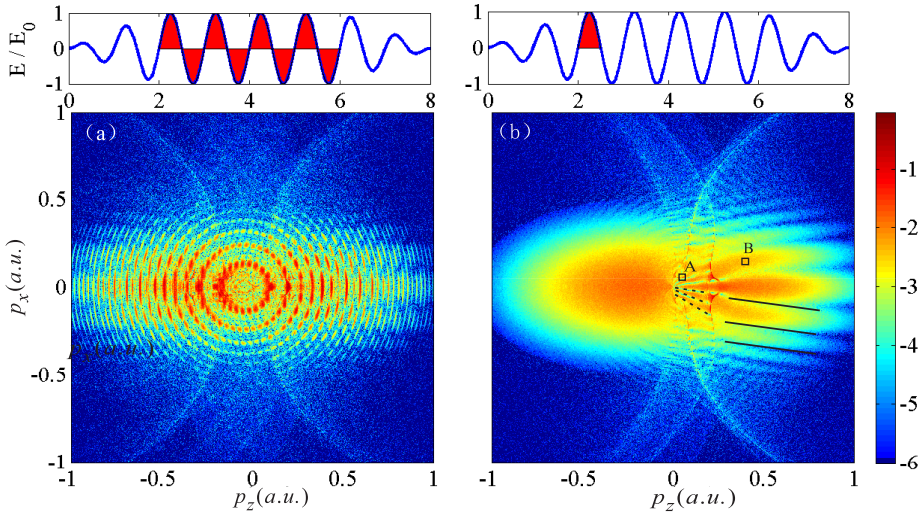

Fig. 1. Two-dimensional PADs of H atoms ionized by an eight-cycle pulses as shown by the top panel using the QTMC model. Red area in electric fields on the top of PADs are the electron ionization time windows for (a) four cycles pulse (b) half-cycle pulse. The dash lines in (b) are used to guide the inner spider structure and the solid lines are used to guide the primary spider structure. The structures A and B show parts of electrons in the lower-energy region ($0 < p_z < 0.32$ a.u.) and higher-energy region ($p_z > 0.32$ a.u.), respectively.

interferences. One can see that the PADs show distinct spider-like structures for the positive momentum, which come from the interferences between the indirect trajectory and the forward scattering trajectory [37]. One can also see that the inner spider structures for [0, 0.32] a.u. and the primary spider structure for [0.32, 1] a.u. are different. The spacing for the lower-energy photoelectron interference patterns along the transversal momentum p_x are smaller than that of the higher-energy photoelectrons, which are guided by the dashed lines and solid lines, respectively (corresponding to the inner and primary spider structures). This agrees well with the experimental observation in [43].

As seen in Fig. 1(b), both the lower-energy photoelectron and higher-energy photoelectron reveal spider-like structures, e.g., the constructive interference patterns along the p_x axis. In order to see which trajectories have a contribution to the inner spider and primary spider structures, we trace back the electron trajectories from one of the interference maximum of the inner-spider and primary-spider structures to the initial tunneling coordinates, i.e., the ionization time and the initial transverse momentum, by using the QTMC model. For simplicity, we will focus on the structures A and B shown in Fig. 1(b), corresponding to the lower-energy electron and higher-energy electron, respectively. Figures 2(b) and 2(c) show the ionization probability with respect to the ionization time and the initial transverse momentum corresponding to area A and area B of Fig. 1(b), respectively. The color bar in Figs. 2(b) and 2(c) indicates the relative contribution of different trajectories. In Fig. 2(b) we can find that four groups of electrons marked as I-IV with different initial conditions have a considerable contribution to the area A of Fig. 1(b). The ionization time of those four groups of electrons are very similar, which are all near the peak of the electric field at about $2.25T$. The initial transverse momenta for areas I-IV are very different, though their final transverse momenta are the same. For the electrons in group I, they are ionized with an initial transverse momentum of ~ 0.22 a.u., which is the same direction as the

Optics EXPRESS

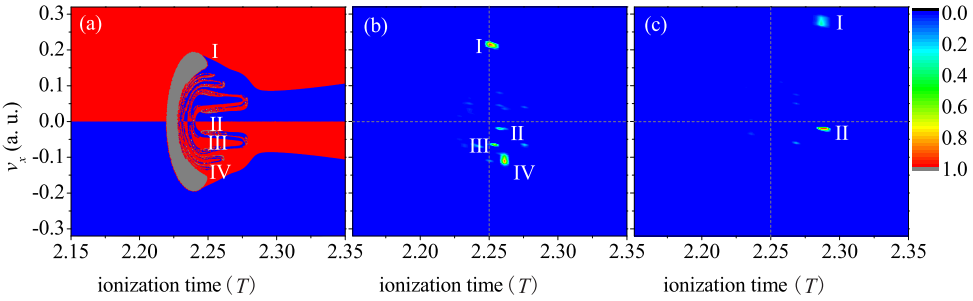

Fig. 2. (a)The electron final transverse momentum with respect to initial transverse momentum and the electron ionization time. Red color represents positive final transverse momentum, blue color represents negative final transverse momentum, and gray color represents unionized electrons (frustrated tunneling ionization). The ionization probability is not included in (a). Panels (b) and (c) show the density plots of the ionization probability with respect to the initial transverse momentum and the ionization time corresponding to the area A and area B in Fig. 1(b), respectively. I represents the indirect trajectory, and II-IV represent different forward scattering trajectories (see text for details).

final transverse momentum (~ 0.15 a.u.). For the electrons in group II, III, and IV, their initial transverse momenta are all negative (nearly -0.02 a.u., -0.06 a.u., and -0.1 a.u., respectively), which is opposite to the final transverse momentum. Because there is no laser field component in the transverse direction, the change of the transverse momentum comes from the effect of the Coulomb potential and the rescattering process. As we will show below, the electrons in groups II, III, and IV come from multiple forward scattering. The case for the higher-energy photoelectrons in area B is different from the LES. In Fig. 2(c), we show the ionization probability with respect to the ionization time and the initial transverse momentum for the area B of Fig. 1(b). One can see that only two groups of photoelectrons will contribute to the final electron momentum distribution, marked as I and II, respectively. Both groups of electrons are ionized at the laser phase of $2.29T$, which is away from the field maximum. The initial transverse momenta of area I and II in Fig. 2(c) are ~ 0.27 a.u. and ~ -0.02 a.u., respectively.

As well known, if neglecting the influence of Coulomb potential effect on the electron motion after the ionization, the transverse momentum will retain its value in the subsequent evolution. To see how the Coulomb potential influences the transverse momentum, we show the electron final transverse momentum (color scale) with respect to initial transverse momentum and the electron ionization time in the combined laser and Coulomb fields in Fig. 2(a). Here the ionization probability is not included. In Fig. 2(a), the red color represents trajectories with positive final transverse momenta and the blue color represents trajectories with negative final transverse momenta. The gray area indicates the electrons recaptured by the ionic potential [48]. For those electrons, they are trapped by the nucleus and can be stabilized in the Rydberg states with negative final energy. One can see that Fig. 2(a) reveals many fractal structures at the laser field maximum ($2.25T$) due to the strong Coulomb effect. Those electrons released near the field maximum will contribute to the LES because $p_f \sim -A(t_0)$, p_f is the final momenta of the electron ionized at t_0. Those fractal structures correspond to the electron scatters many times by the nucleus with low impact parameter and, as a result, shows chaotic behavior. The electrons with chaotic dynamics have minor effects on the LES [19]. Beside these fractal structures, one can see many island-like structures, e.g., marked by II, III, and IV in red area. To see how these island-like structures come from, for simplicity, we focus on the electrons with positive final transverse momentum (red color). One can see that most of them are contributed by the elec-

Optics EXPRESS

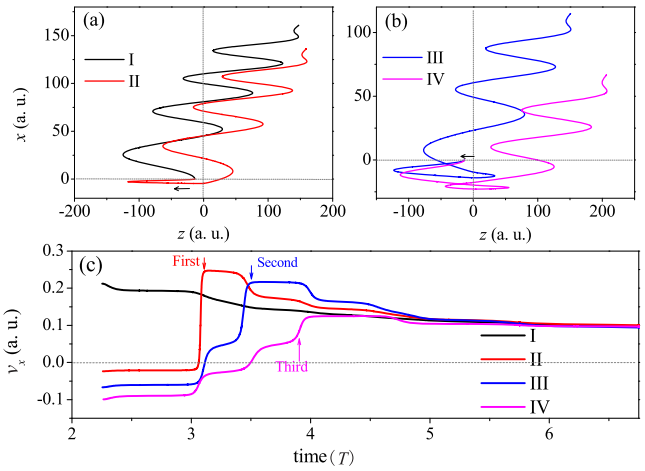

Fig. 3. Panels (a) and (b) show the typical trajectories of I-IV in Fig. 2(b) using the QTMC model. (c) The electrons transverse momenta evolution corresponding to the four trajectories in (a) and (b). I is the indirect electron and II III and IV stand for the single, double and triple forward scattering electrons, respectively. z is the laser polarization direction and x is the transverse direction. All the trajectories have the same final momentum.

trons with positive initial transverse momentum (indicated by I), which are the nonscattering trajectories. After the field maximum, one can see that some area with negative initial transverse momentum will also contribute to the electrons with positive final transverse momentum. For the ionization occurs within $[2.28T, 2.35T]$ (corresponding to the higher electron energy), there is only one group of electrons with negative initial transverse momenta from -0.1 a.u. to zero. For the ionization occurs within $[2.25T, 2.28T]$ (corresponding to the lower electron energy), there are three groups of electrons with different initial transverse momenta. The initial transverse momenta of these three groups are nearby -0.02 a.u., -0.06 a.u. and -0.1 a.u. (marked as II, III and IV), respectively. Those groups of electrons agree well with those in Figs. 2(b) and 2(c). This means that those groups of electrons are contributed by different rescattering processes. The back analysis of initial tunneling coordinates of the low-energy electrons with consideration of the Coulomb potential provides very sophisticated information.

To further show the origin of those groups of electrons, we trace the trajectories of the electrons using QTMC model. In Fig. 3, we show the typical trajectories and the time evolution of the transverse momentum corresponding to the four groups of electrons in Fig. 2(b). Their final momenta are ~ 0.22 a.u. for p_z and ~ 0.12 a.u. for p_x. For trajectory I, it can be driven back in the laser polarization direction (z axis) without rescattering due to the large transverse distance (larger than 50 a.u.) at its return. Thus, trajectory I belongs to the indirect trajectory. For trajectory II, the electron with small negative initial momentum is driven back by the laser field and a single forward rescattering occurs $\sim 0.75T$ after the ionization as seen in Fig. 3(c). For trajectory III, the tunneled electron experiences a double forward rescattering process. For this trajectory, the initial transverse momentum is almost -0.06 a.u., the electron lateral distance to the nucleus is large at its first return and the Coulomb potential merely focus the electrons indirectly to the nucleus. As a result, the forward scattering happens $\sim 0.75T$ and $\sim 1.25T$ after the ionization when the electron returns to the nucleus. Similarly, trajectory IV scattered with the nucleus three times $\sim 0.75T$, $\sim 1.25T$ and $\sim 1.75T$ after the ionization with nearly the same change of the transverse momentum, as seen in Fig. 3(c).

Obviously, the number of the rescattering depends on the initial transverse momenta. For

Optics EXPRESS

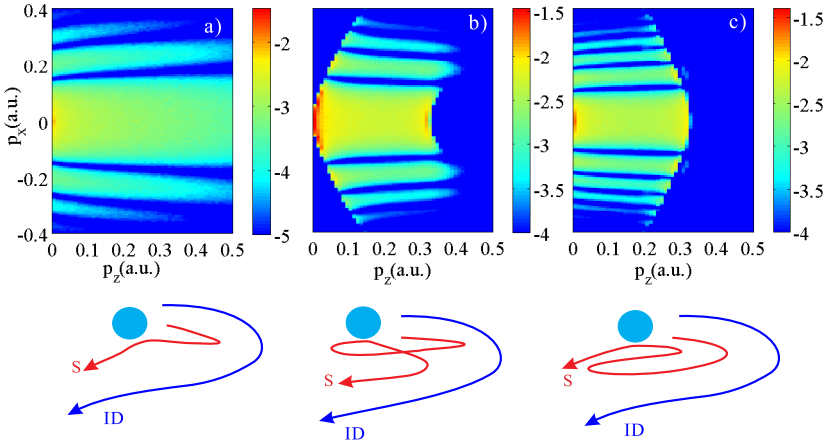

Fig. 4. (a)-(c) are the interference patterns from the interference between indirect trajectory and the single, double and triple-scattered trajectory using the semi-classical recollision model, respectively. The relative contributions of each interference pattern are not included. The schematic diagrams on the bottom row illustrate the indirect trajectory (ID) and the forward rescattering trajectories (S).

trajectory I, the electron has a large initial transverse momentum of $\sim$ 0.3 a.u., and it returns to the nucleus along the polarization direction with a large lateral distance. Thus, the value of the transverse momentum slightly decreases under the influence of the Coulomb focusing effect. Trajectory II rescatters off the nucleus once because it has a very small initial transverse momentum of -0.02 a.u., showing a jump of the transverse momentum at $\sim 3T$ in Fig. 3(c) at the instant of the rescattering. Trajectory III has an initial transverse momentum of -0.06 a.u. and it scatters at $\sim 3T$ and $\sim 3.5T$. Because of the largest initial transverse momentum of ~ -0.1 a.u., trajectory IV exhibits jump of the electron transverse momentum at $\sim 3T$, $\sim 3.5T$ and $\sim 4T$, which means that it scatters with the nucleus three times. From Figs. 2 and 3, one can see that the scattering leads to sign-reversal of the transverse momentum of the classical trajectories.

We then study the relative contributions of those trajectories to the photoelectron angular distributions. For the low-energy region (p_z < 0.32a.u.), we can find that the ionization probability of trajectories I and IV is much larger than that of trajectories II and III, as seen in Fig. 2(b). Thus, the interference between the trajectories I and IV corresponds to the inner spider structure in the low-energy region of Fig. 1(b). As seen in Fig. 3(c), one can see that the change of transverse momenta becomes smaller from trajectory II to trajectory IV at the scattering. The slight change of the transverse momentum for the triple-scattered trajectory means a small scattering angle at the rescattering. Because of the smaller scattering angle, the scattering cross section of the triple-scattered trajectory is correspondingly larger than that of the single-scattered and double-scattered trajectory. Thus, the contribution of the triple-scattered trajectory is dominant over the single-scattered and the double-scattered trajectory for the low-energy photoelectrons. In the low-energy region, the inner spider interference patterns are dominated by the interference of the nonscattering trajectory and the triple forward scattering trajectories. For high-energy photoelectrons (p_z > 0.32a.u.), we can only find the groups I and II in Fig. 2(c). As a result, the interference between the trajectories I and II corresponds to the primary spider structure in the high-energy region of Fig. 1(b).

To further study the Coulomb effect on the interference patterns, we use the semi-classical rescattering model to simulate the interference patterns among those forward scattering trajecto-

Optics EXPRESS

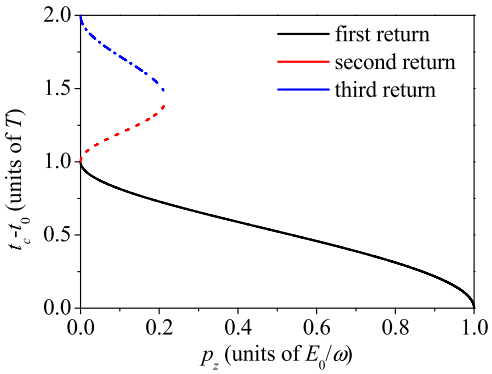

Fig. 5. The time difference between the rescattering and the ionization with respect to the final momentum p_z, for the single (solid), double (dashed) and triple (dot dashed) forward scattering trajectories, respectively.

ries and the nonscattering trajectories. Figures. 4(a)-4(c) show the interference patterns among the indirect trajectory and the single, double and triple forward scattering trajectory, respectively. The interference structure in Fig. 4(a) shows no cutoff when p_z is smaller than 0.5 a.u. In Fig. 4(b), we can find two cut-offs in the interference pattern at $0.092U_p$ (p_z = 0.32 a.u.) and 0 which is caused by the double forward scattering electron. All those cut-offs agree well with Fig. 1(b), though the long-range Coulomb potential is neglected in the rescattering model. When electron with single or triple forward scattering trajectory, the interference between the indirect trajectory and the scattering trajectory reveals an interference structure which becomes narrow with decreasing the longitudinal momenta, as seen in Figs. 4(a) and 4(c). But in Fig. 4(b) the interference between the indirect trajectory and the double forward scattering trajectory reveals an interference structure which becomes narrow with increasing the longitudinal momenta.

Comparing the interference patterns in Figs. 4(a) and 4(c) with those in the low-energy region (p_z < 0.32 a.u.) and high-energy region (p_z > 0.32 a.u.) of Fig. 1(b), respectively, one can see that the long-range Coulomb potential has a crucial effect on the low-energy photoelectron interference patterns, as compared with the high-energy electrons. When considering the long-range Coulomb potential, the interference patterns is nearly unchanged for the high-energy photoelectron with p_z > 0.32 a.u., while the inner spider structure (p_z < 0.32 a.u.) becomes narrower for lower longitudinal momenta and it converges to zero momentum with the consideration of the Coulomb effect, when comparing Fig. 1(b) with Fig. 4(c). For the multiple forward scattering trajectory, because the electron will not be too far away from the nucleus before the scattering ended, the Coulomb potential will have a large impact on the trajectory all the time. As seen in Fig. 3(c), the transverse momentum of the triple-scattered trajectory is greatly changed by the long-range Coulomb potential before the rescattering at $4T$. Due to the larger Coulomb focusing, there are more triple-scattered trajectories contributing to the lower-energy photoelectrons. Thus the interference of the indirect trajectory and the triple forward scattering trajectory will play the most significant role in the low-energy region, as seen in Fig. 1(b) and Fig. 2(b).

Furthermore, the interference patterns have encoded the temporal information of the rescattering trajectories. From Eq. (9), the phase difference between the forward scattering and nonscattering trajectories is mainly determined by $-\frac{1}{2}p_x^2(t_c - t_0)$, because the ionization time of the scattering trajectory and the nonscattering (indirect) trajectory is nearly the same. For a specific interference stripe in Fig. 4, the phase difference keeps nearly unchanged. With increasing p_x^2, the time difference between the rescattering and the ionization ($t_c - t_0$) will decrease, thus the bending direction of the stripe is along the decreasing direction of the time difference. In Fig. 5,

Optics EXPRESS

we show the time difference between the rescattering and the ionization with respect to the final momentum p_z. For trajectory II (solid) and IV (dot dashed), the time difference decreases with the increase of the final momentum p_z , thus the interference fringes become narrower for lower longitudinal momenta in PADs. For trajectory III (dashed), the time difference increase with the increase of the final momentum p_z, thus the interference structures become narrower for higher longitudinal momenta, which agrees well with the interference patterns shown in Fig. 4. Moreover, the fringe spacing also depends sensitively on this time difference. The much longer time difference for trajectory III and IV leads to much smaller fringe spacing, as seen in Figs. 1 and 4.

4. Conclusion

In conclusion, we have systematically studied the intra-half-cycle interference of an atom ionized by a mid-infrared laser field. Our study reproduces the experimentally observed inner spider structure in the low-energy regions of the PADs [43], which comes from the intra-half-cycle interference of multiple forward scattering electron wave packet and nonscattering electron wave packet. With tracing back to the initial tunneling coordinates, we find that up to three kinds of forward scattering trajectories have a substantial contribution to the low-energy photoelectrons. Depending on the initial transverse momentum at the tunnel exit, those multiple forward scattering trajectories will interfere with the nonscattering trajectories. Those rescattering trajectories will reverse the transverse momentum of the electrons. We identify that the interference between the nonscattering trajectory and the triple-scattered trajectory has the largest contributions to the low-energy photoelectrons in a mid-infrared laser field. Comparing the QTMC model with the semi-classical rescattering model, we show that the long-range Coulomb potential will change the shape of the intra-half-cycle interference fringes in the low-energy region, but it has little effect on the low-energy cut-offs. Under the influence of the long-range Coulomb potential, the low-energy electron intra-half-cycle interference stripes converge to zero momentum with the decrease of the photoelectron longitudinal momentum. We also show the intra-half-cycle interference has stored the temporal information, i.e., the time difference between the rescattering and the ionization. This study provides fruitful information for the low-energy photoelectron interference and it provides an alternative way to probing the time-resolved electron dynamics.

Funding

National Natural Science Foundation of China (61405064 and 11234004); Fundamental Research Funds for the Central University (HUST: 2016YXMS012).